This is section 2
of Chapter II of
AFWL-TR-68-7 Vol I

CORRECTION MADE ON PG. 8
FORMULA (23)

EMP Interaction Notes

Note VIII
June 1967

Internal Voltages and Currents in Complex Cables

E. F. Vance

Stanford Research Institute
Menlo Park, California

Abstract

Techniques for computing the internal currents and voltages in cables having one or more shields when the outer shield is driven are described. Computed results are given for an example cable for which experimental data are available.

I INTRODUCTION

Analytical techniques for determining the current induced in long conductors near the surface of the ground by surface fields have been developed by Sunde[1]* and Wait.[2] These techniques have been verified for insulated and bare conductors in experiments conducted with a CW transmitter, and computer programs have been developed to calculate the currents using a version of Sunde's theory.[3,4] Until recently, however, cable-current theory was limited to determining the total current induced in a cable. Nevertheless, for many applications where shielded or multiply shielded cables are used, it is important to know what voltages and currents are induced in the signal-carrying core of the cable. The purpose of this note is to describe one technique that has been developed to compute these internal currents and voltages.

The technique described here combines the shielding theory of Kaden[5] and the transmission-line theory of Sunde. Classical shielding theory is used to determine the axial electric-field strength at the inside surface of the shield from the current flowing in the shield. This axial electric field is then used in the transmission-line equations for a line with a distributed driver to compute the current in the core and the core-to-shield voltage. (In the case of multiple shields, multiple applications of these two steps are required to progress from the outer shield through the inner shields to the core.)

In the following analysis, it is assumed that the shields are good conductors ($\sigma \gg \omega\varepsilon$), that the diameter of the cable is small compared to the shortest wavelength of interest, and that the current is uniformly distributed over the circumference of the cable. It is also assumed that the coupling between the core or inner shields and the outer shield is loose, so that variations in the interior currents (due to differences in the terminations or to standing waves on inner shields or core wires) do not cause significant changes in the total cable current. This restriction, although seemingly severe, does not impose a significant

*References are given at the end of this note.

limitation for most practical shielded-cable configurations, in which over 90 percent of the total current flows in the outer shield. Finally, only solid shields of circular cross section are considered in this note. The same general approach can be used for other types of shields (e.g. braids) providing the transfer impedance for these shields can be obtained.

II TRANSFER IMPEDANCE

All of the properties of cylindrical conductors that are important in this analysis can be obtained from the analysis of a cylindrical tube. We are concerned here with axially directed electric fields and conductors that support only the TEM modes of propagation. We assume that the conductor diameter is smaller than the smallest wavelength of interest, and that radiation from the conductor can be neglected. Considering first a tubular conductor driven at its outside surface, the electric and magnetic fields in the conductor are obtained from

$$\nabla^2 E_x = j\omega\mu(\sigma + j\omega\varepsilon)\, E_x \quad , \qquad \nabla \times E = -j\omega\mu H \quad . \tag{1}$$

Solution of these equations, subject to the conditions that $E_x = E_0$ at the outside surface and $H_\Phi = 0$ at the inside surface, gives

$$E_x = E_0 \left[\frac{H_1^{(1)}(\rho_i)\, J_0(\rho) - J_1(\rho_i)\, H_0^{(1)}(\rho)}{H_1^{(1)}(\rho_i)\, J_0(\rho_0) - H_0^{(1)}(\rho_p)\, J_1(\rho_i)} \right] \tag{2}$$

and

$$H_\Phi = \frac{\sigma E_0 r}{\rho} \left[\frac{H_1^{(1)}(\rho_i)\, J_1(\rho) - J_1(\rho_i)\, H_1^{(1)}(\rho)}{H_1^{(1)}(\rho_i)\, J_0(\rho_0) - H_0^{(1)}(\rho_0)\, J_1(\rho_i)} \right] \tag{3}$$

where

$\delta = (\pi f \mu \sigma)^{-1/2}$

$\rho = -(1 - j)\, r/\delta$, r = distance from axis of tube

$\rho_0 = -(1 - j)\ r_0/\delta r_0$ = radius of outside surface

$p_i = -(1 - j)\ r_i/\delta r_i$ = radius of inside surface

and $J_n(\rho)$ and $H_n^{(1)}(\rho)$ are Bessel functions of the first kind and Hankel functions of the first kind, respectively, of order n.

The electric field on the inside surface of the tube may be obtained directly from Eq. (2) by letting $\rho = \rho_i$. It will be more useful in the induced-current analysis, however, to determine the field inside the tube in terms of the current in the tube. This current is

$$I = 2\pi r_0\ H_\Phi(\rho) \tag{4}$$

so that

$$\frac{E_x(\rho_i)}{I} = -\frac{1 - j}{2\ \pi r_0 \sigma\delta}\left[\frac{H_1^{(1)}(\rho_i)\ J_0(\rho_i) - H_0^{(1)}(\rho_i)\ J_1(\rho_i)}{H_1^{(1)}(\rho_i)\ J_1(\rho_0) - H_1^{(1)}(\rho_0)\ J_1(\rho_i)}\right] . \tag{5}$$

It is noted that in the limit as $\rho_i \to 0$ and $\rho_0 \to 0$ with ρ_0/ρ_i constant, the ratio of the axial field to the total current approaches

$$\left.\frac{E_x(\rho_i)}{I}\right|_{dc} \approx -\frac{1 - j}{2\ \pi r_0 \sigma\delta}\left[\frac{2r_0\delta}{-(1 - j)(r_0^2 - r_i^2)}\right] = \frac{1}{\pi\sigma(r_0^2 - r_i^2)} \tag{6}$$

which is recognized as the dc resistance per unit length of the tube. For the high-frequency case ($\rho_i \gg 1$, $\rho_0 \gg 1$)

$$\left.\frac{E_x(\rho_i)}{I}\right|_{HF} \approx -\frac{1 - j}{2\ \pi r_0 \sigma\delta}\left[-j\sqrt{\frac{r_0}{r_i}}\ 2e^{-(1+j)}\ \frac{(r_0 - r_i)}{\delta}\right]$$

$$= \frac{1 + j}{\pi r_0 \sigma\delta}\sqrt{\frac{r_0}{r_i}}\ e^{-(1+j)}\ \frac{r_0 - r_i}{\delta} . \tag{7}$$

If $\sqrt{r_0/r_i} \approx 1$ and $r_0 - r_i = T$, Eq. (7) is identical to the solution obtained for a thin sheet of width $2\pi r_0$.

For many cable configurations $T/r_0 \ll 1$, and plane-wave theory is applicable. Since the Bessel and Hankel functions of the cylindrical-wave theory are more time-consuming to compute for large arguments, it is convenient to use the plane-wave solutions when permissible. The plane-wave theory gives

$$\frac{E_x(T)}{I} \approx \frac{1 + j}{2\pi r_0 \sigma \delta} \left(\frac{1}{\sinh \Gamma T} \right) \tag{8}$$

where

$$\Gamma = [j\omega\mu(\sigma + j\omega\epsilon)]^{1/2} \quad . \tag{9}$$

A plot of the normalized transfer-impedance magnitude and its phase, obtained from the plane-wave solution, is shown in Fig. 1. Also shown in Fig. 1 are the high-frequency and low-frequency approximations to the transfer impedance.

III TRANSMISSION LINE WITH DISTRIBUTED SOURCE

The analysis of the transmission line with a distributed driving source is similar to that of the more conventional transmission line with lumped sources, except for the source term. For the transmission line with a distributed driving source -E per unit length, the voltage drop is given by

$$\frac{dV}{dx} = E - IZ \tag{10}$$

where Z is the impedance per unit length of the line. The line current is

$$\frac{dI}{dx} = -VY \tag{11}$$

where Y is the admittance per unit length of the line. (Formulas for the impedance and admittance are given in the Appendix.) Differentiating (11) and substituting in (10) gives the second-order differential equation for the current in the transmission line:

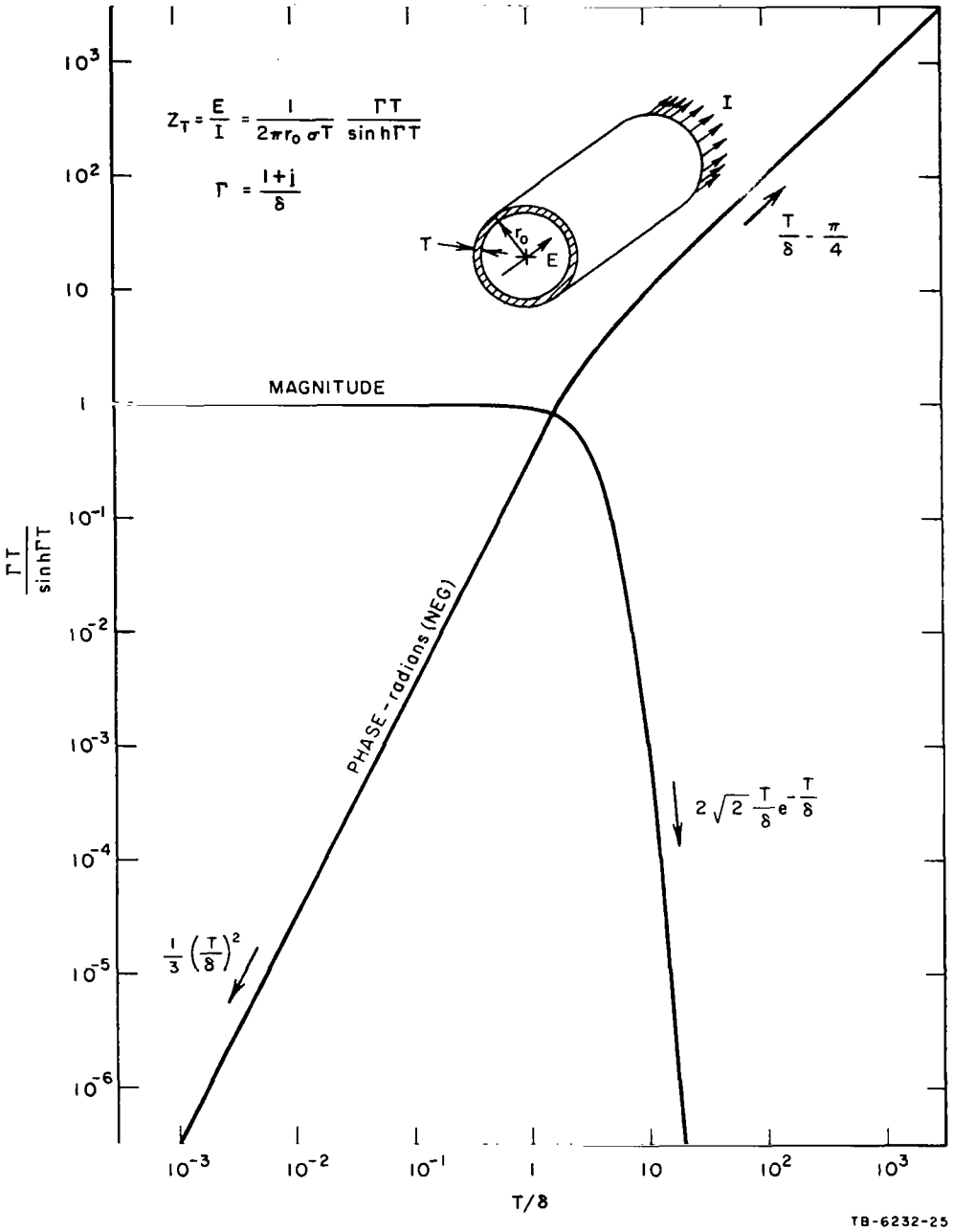

FIG. 1 NORMALIZED TRANSFER IMPEDANCE FOR THIN-WALLED SOLID CYLINDRICAL SHIELDS

$$\frac{d^2I}{dx^2} - \gamma^2 I = -YE \tag{12}$$

where $\gamma^2 = ZY$.

The solution of Eq. (12) for the current I is of the form

$$I = K_1 e^{\gamma x} + K_2 e^{-\gamma x} + F(x,\omega) \tag{13}$$

where

$$F(x,\omega) = -\frac{1}{2Z_0}\left[e^{\gamma x}\int e^{-\gamma x}\, E\, dx - e^{-\gamma x}\int e^{\gamma x}\, E\, dx\right] \tag{14}$$

$$Z_0 = \sqrt{Z/Y}$$

and K_1 and K_2 are arbitrary constants.

Substituting (13) into (11) the line voltage is obtained:

$$V = -Z_0\left[K_1 e^{\gamma x} - K_2 e^{-\gamma x} + F_v(x,\omega)\right] \tag{15}$$

where

$$F_v(x,\omega) = \frac{1}{\gamma}\left[\frac{\partial F(x,\omega)}{dx}\right] \tag{16}$$

From Eqs. (13) through (16) and the boundary conditions (terminating impedance) the constants K_1 and K_2 can be evaluated, and the line current and voltage can then be evaluated from Eqs. (13) and (14). Thus for a line extending from x = a to x = b and terminating in $Z_a = z_a Z_0$ at x = a and $Z_b = z_b Z_0$ at x = b,

$$V(a) = -I(a)Z_a \qquad V(b) = I(b)Z_b \tag{17}$$

and

$$K_1 = \frac{e^{-\gamma b}(1 - z_b)\left[F_v(a) - z_a F(a)\right] - e^{-\gamma a}(1 + z_a)\left[F_v(b) + z_b F(b)\right]}{e^{\gamma(b-a)}(1 + z_a)(1 + z_b) - e^{-\gamma(b-a)}(1 - z_a)(1 - z_b)} \quad (17)$$

$$K_2 = \frac{e^{\gamma b}(1 + z_b)\left[F_v(a) - z_a F(a)\right] - e^{\gamma a}(1 - z_a)\left[F_v(b) + z_b F(b)\right]}{e^{\gamma(b-a)}(1 + z_a)(1 + z_b) - e^{-\gamma(b-a)}(1 - z_a)(1 - z_b)} \quad . \quad (18)$$

The form of $F(x,\omega)$ given above is useful if the driving field $E(x,\omega)$ is of such a form that the indicated indefinite integrals can be evaluated. Where numerical integration is necessary to evaluate the integrals, however, it is more convenient to use the definite-integral form

$$F(x,\omega) = \frac{1}{2Z_0} \int_a^b e^{-\gamma|x-v|} E(v,\omega)\, dv \quad . \quad (19)$$

IV IMPULSE RESPONSE

The response of the interior of the cable to a unit impulse of current on the exterior shield is of particular interest, since this response gives an indication of the effectiveness of the shielding system in preventing energy from being coupled into the interior. The unit impulse propagating with velocity ω/k on the outer shield is

$$I(x,t) = \delta\left(t - \frac{kx}{\omega}\right) \quad (20)$$

In the frequency domain, this propagating pulse is represented by

$$I(x,\omega) = e^{jkx} \quad . \quad (21)$$

Since the axial field inside the shield depends only on the local shield current, this field is

$$E(x,\omega) = Z_T\, e^{jkx} \quad (22)$$

where Z_T is the transfer impedance given in Eq. (8). The current in the inner shield (or core) is thus given by Eq. (13), where

$$F(x,\omega) = -\frac{e^{jkx}}{2Z_0}\,\frac{2\gamma}{k^2+\gamma^2}\,Z_T \quad . \tag{23}$$

V COMPUTED RESULTS (IMPULSE RESPONSE)

The techniques described in Secs. II and III were used to compute the properties of a doubly shielded cable having a 20-mil copper outer shield, a 10-mil mild-steel inner shield, and a core comprised of 8 pairs of 16-gauge copper and 18 pairs of 19-gauge copper. A cable length of 640 meters (2100 ft) was chosen, since this length of cable had been used in experiments in which some of the computed properties were measured. The cable shields were assumed to be shorted at the ends, and the core-to-inner shield termination was assumed to be open-circuited. Other properties of the cable are given in Table I.

Table I

PROPERTIES OF EXAMPLE CABLE

Characteristic	Outer Sheath	Gap	Inner Sheath	Gap	Core
Material	copper	air, polyethylene	mild steel	polyethylene	copper
Radius (cm)	2.2	-	1.5	-	1.0
Thickness (mils)	20	-	10	-	
Conductivity* (mho/m)	4.7×10^7	0	7.5×10^6	0	5.8×10^7
Relative Permeability	1.0	1.0	620	1.0	1.0
Dielectric Constant	10	1.4	10	2	10

*The reduced conductivity of the outer sheath was used to accommodate the fact that the outer sheath was corrugated.

The magnitudes of the transfer impedances computed from Eq. (8) are shown in Fig. 2 for this cable. As is apparent from Fig. 2, the corner

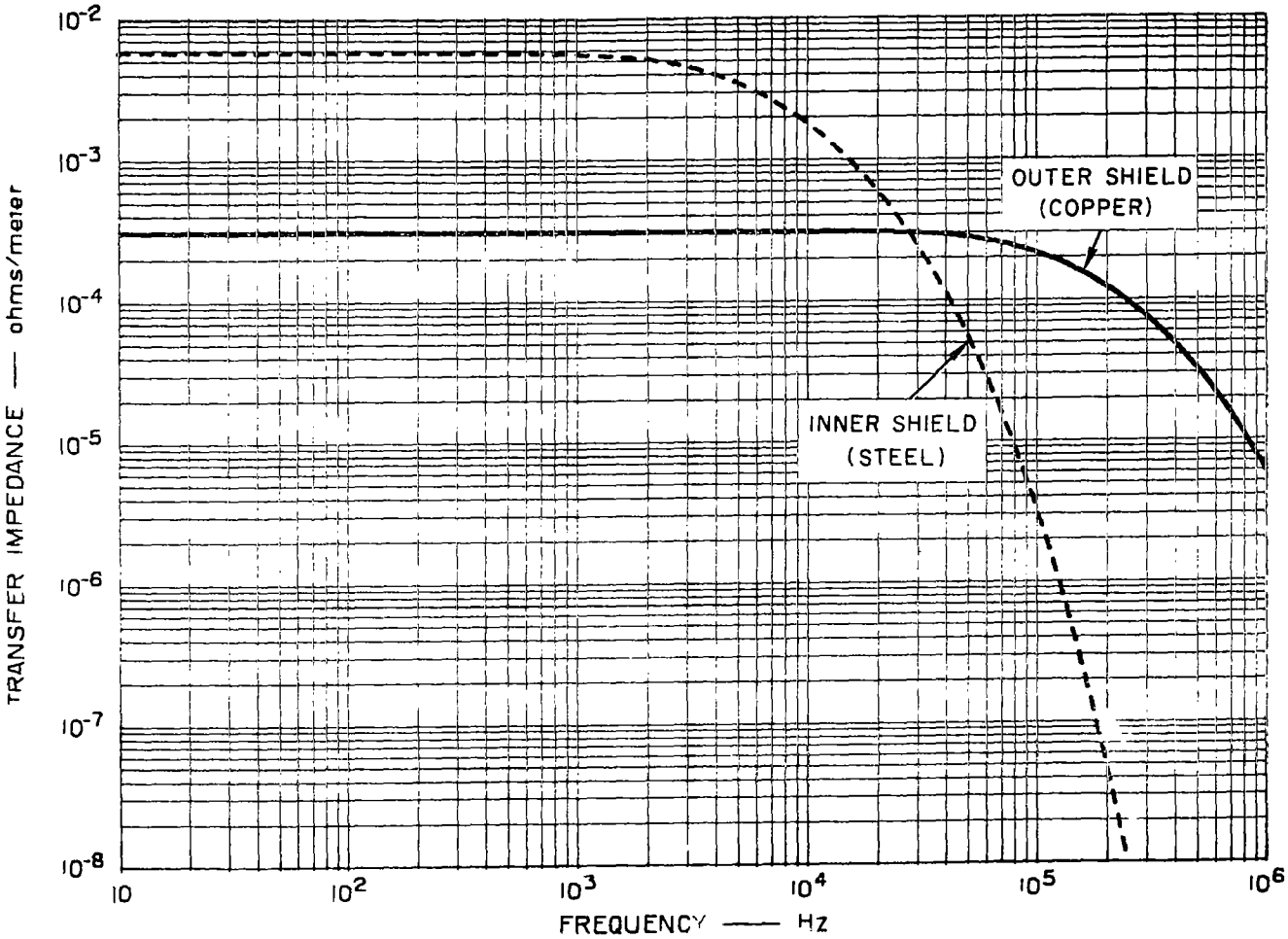

FIG. 2 MAGNITUDE OF TRANSFER IMPEDANCE FOR 20-mil COPPER SHIELD AND 10-mil MILD-STEEL SHIELD

frequency (3 dB point) for the 20-mil copper sheath is at 110 kHz, while the corner frequency for the mild-steel inner sheath is at 4 kHz. Above the corner frequencies the transfer impedances decrease exponentially, and very little axial field is produced at the inside surface of the shields by currents impressed on the shield. Below the corner frequency, the transfer impedance is relatively independent of frequency, and the axial field at the inside surface is essentially the same as the axial field at the outside surface.

The response of the current in the inner shield to a unit impulse current in the outer shield is given by the solid curve in Fig. 3. Note that because of short-circuit termination between the inner and outer shields, the current in the inner shield is a fixed fraction of the total current at low frequencies, where the impedances of the copper and steel sheaths are essentially the dc resistances of the shields. At approximately 500 Hz, however, the impedance of the steel sheath begins to deviate significantly from the dc value because of skin effect in the permeable steel. The fraction of the total current that flows in the inner shield thereafter decreases with increasing frequency up to 200 kHz, where the first resonance effects are noted. The peak of the first resonance is 40 dB below the low-frequency response, however, so that it does not influence pulse shapes significantly for the cable length used in this example. It is interesting to note that even in the low-frequency region, the inner-sheath current is less than 6 percent of the total current, so that the "loose-coupling" assumption is satisfactory. As will be seen later, the current in the inner sheath is the same at all points along the cable except at the high frequencies (above 100 kHz). The dashed curve of Fig. 3 shows the current in the core when a unit impulse of current is applied to the inner shield. To simplify this calculation, the core was assumed to be a solid copper conductor of 1.0 cm radius. Because of the open-circuit termination between core and shield, the core current is zero at the ends of the cable; hence the core current shown in Fig. 3 was computed at the center of the cable where the current is maximum. The line formed by the inner and outer shields and that formed by the core and inner shield differ mainly in

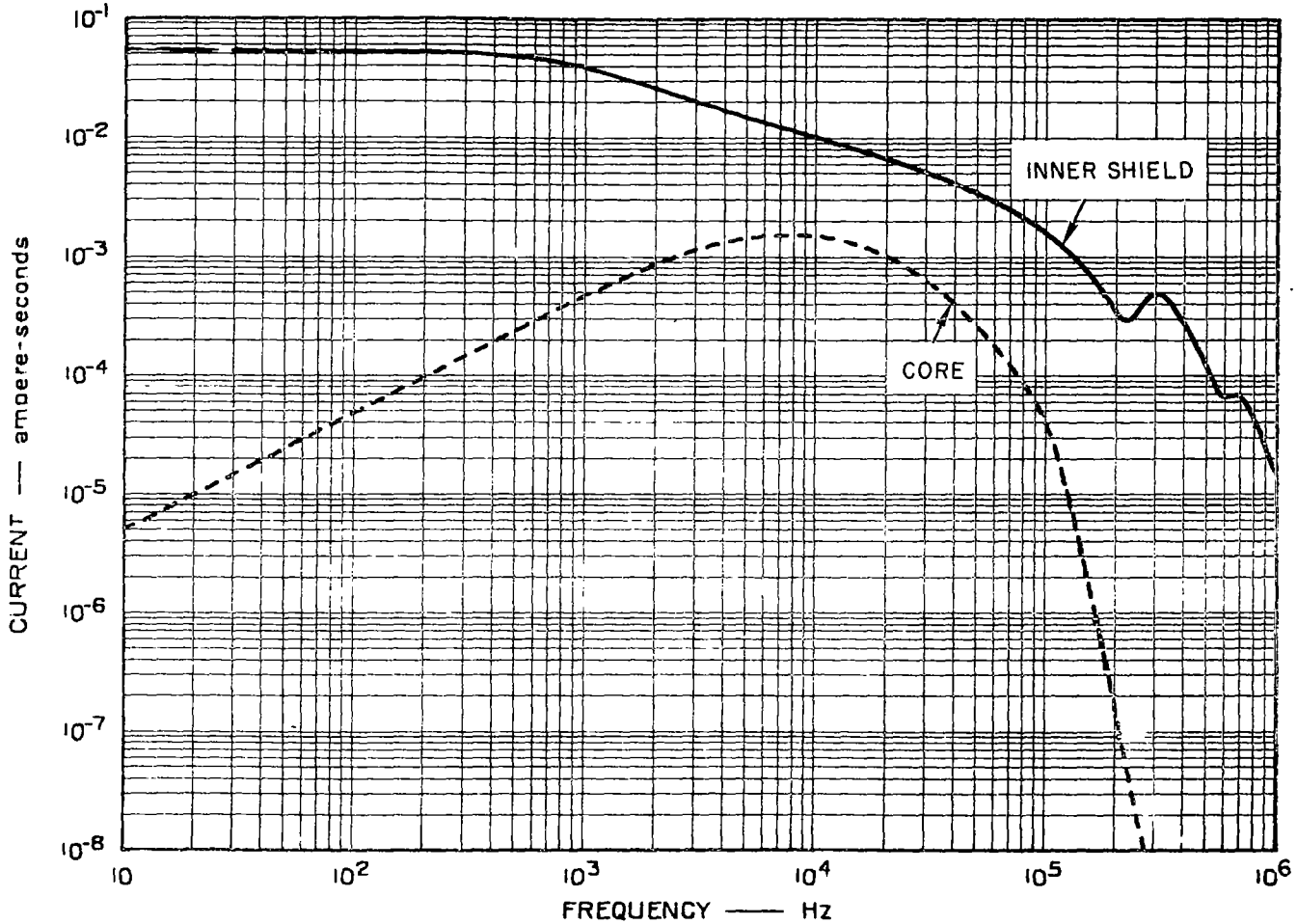

FIG. 3 CURRENT RESPONSES TO UNIT IMPULSE. Solid curve – current in inner shield when current impulse is applied to outer shield. Dashed curve – current in core when current impulse is applied to inner shield.

their terminations. The effect of the steel shield in limiting the current at frequencies above 500 Hz in the line formed by the two shields also causes a difference in the behavior of the lines.

Because of the open-circuit termination, the current in the core is induced by capacitive coupling to the voltage generated in the inner sheath. Hence at frequencies up to a few kHz, the current is directly proportional to frequency. Above a few kHz, however, the shielding effect of the inner sheath becomes significant and the driving field inside the inner shield begins to decrease exponentially (see Fig. 2). Thus the current spectrum in the core has a broad maximum at about 9 kHz.

The internal voltages, computed from Eq. (15), are shown in Fig. 4. The shield-to-shield voltage is computed at the center of the cable where this voltage is maximum, and the core-to-inner shield voltage is computed at the end of the cable, where it is maximum. The same unit impulse of driving current described above was used.

The core-shield voltage curve is very similar to the inner-shield transfer impedance of Fig. 2 (except for some suppressed resonances above 100 kHz). This follows from the fact that the core-shield line is open-circuited at the ends, and the voltage drop along the core is insignificant compared to the voltage generated along the inner sheath. Thus, to a first approximation, the voltage appearing between the core and the inner sheath at the end of the cable is the integrated axial field (along the inner shield) from the midpoint of the cable to that end. For longer cables, however, propagation effects may be significant, and cable resonances may fall within the passband of the inner shield.

The low-frequency shield-to-shield voltage indicated by the solid curve of Fig. 4 is produced by the current flowing through the inductive reactance of the shield-to-shield transmission line short-circuited at its ends. Thus this voltage is proportional to frequency in the low-frequency portion of the spectrum where the driving field (transfer impedance of Fig. 2) and line inductance are constant. Above 100 kHz, the voltage is affected by the shielding of outer shield and by resonances of the short-circuited shields.

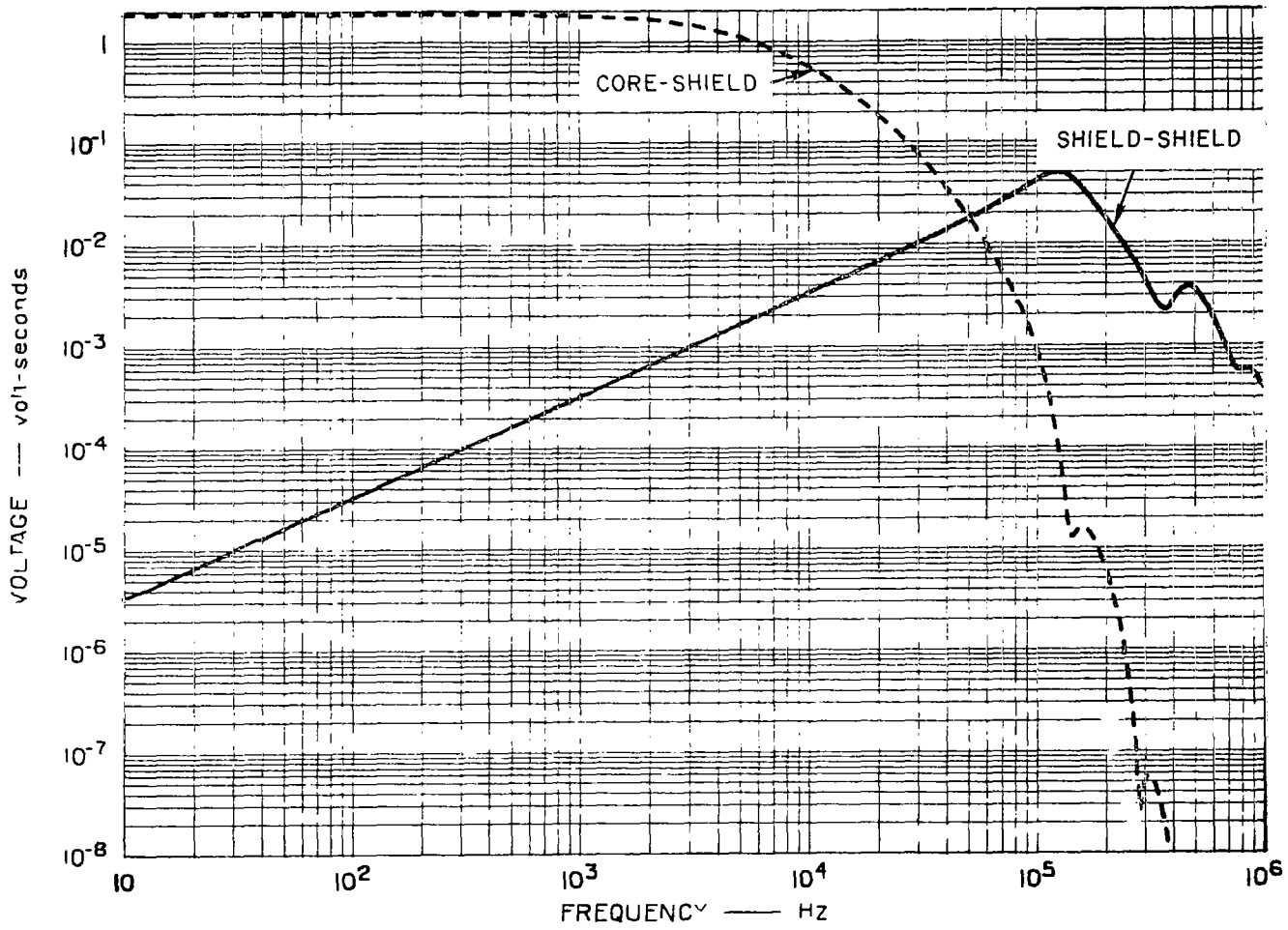

FIG. 4 VOLTAGE RESPONSES TO UNIT IMPULSE. Solid curve – shield-to-shield voltage when current impulse is applied to outer shield. Dashed curve – core-to-shield voltage when current impulse is applied to inner shield.

VI COMPUTED RESULTS (EXPERIMENTAL DRIVER)

Additional computations were also made with a specific driving current in the outer shield. The driving current used for these computations was an analytic representation of the actual driving current used in experiments on the 640m test cable.[6] Experimental data are therefore available for comparison with these computed results.

The driving current in the outer shield was a pulse having a rise time of approximately 150 ns followed by an exponential decay. The time constant for the decay was approximately 150 μs. This current pulse is represented by

$$I(t) = I_0 e^{-\alpha t}(1 - e^{-\beta t}) \tag{24}$$

where $I_0 = 700A$, $\alpha = 6670$, and $\beta = 1.3 \times 10^7$. A plot of this pulse is shown in Fig. 5.

In the frequency domain, the pulse is represented by

$$I(\omega) = I_0\left[\frac{1}{\alpha + j\omega} - \frac{1}{\alpha + \beta + j\omega}\right] \tag{25}$$

which is plotted in Fig. 6. As can be seen in Fig. 6, the spectrum of the pulse is flat out to $f = \alpha/2\pi \approx 1$ kHz, above which the spectrum is inversely proportional to frequency. At $f = (\alpha + \beta)/2\pi \approx 2.1$ MHz, a second corner frequency, associated with the pulse rise-time, occurs.

Since the spectral components of this pulse propogate in the same fashion as the unit impulse, the response of the outer sheath and the outside of the inner sheath to the driver spectrum of Fig. 6 is obtained by multiplying the driver spectrum by the impulse responses of Figs. 3 and 4 (solid curves). The spectra of the current in the inner shield obtained in this manner at five points along the cable are shown in Fig. 7, and the shield-to-shield voltage spectra are shown for the three interior points in Fig. 8 (the voltage at the endpoints is zero because of the short-circuit terminations). As can be seen in Fig. 7, the current spectra are nearly identical at all points along the cable at

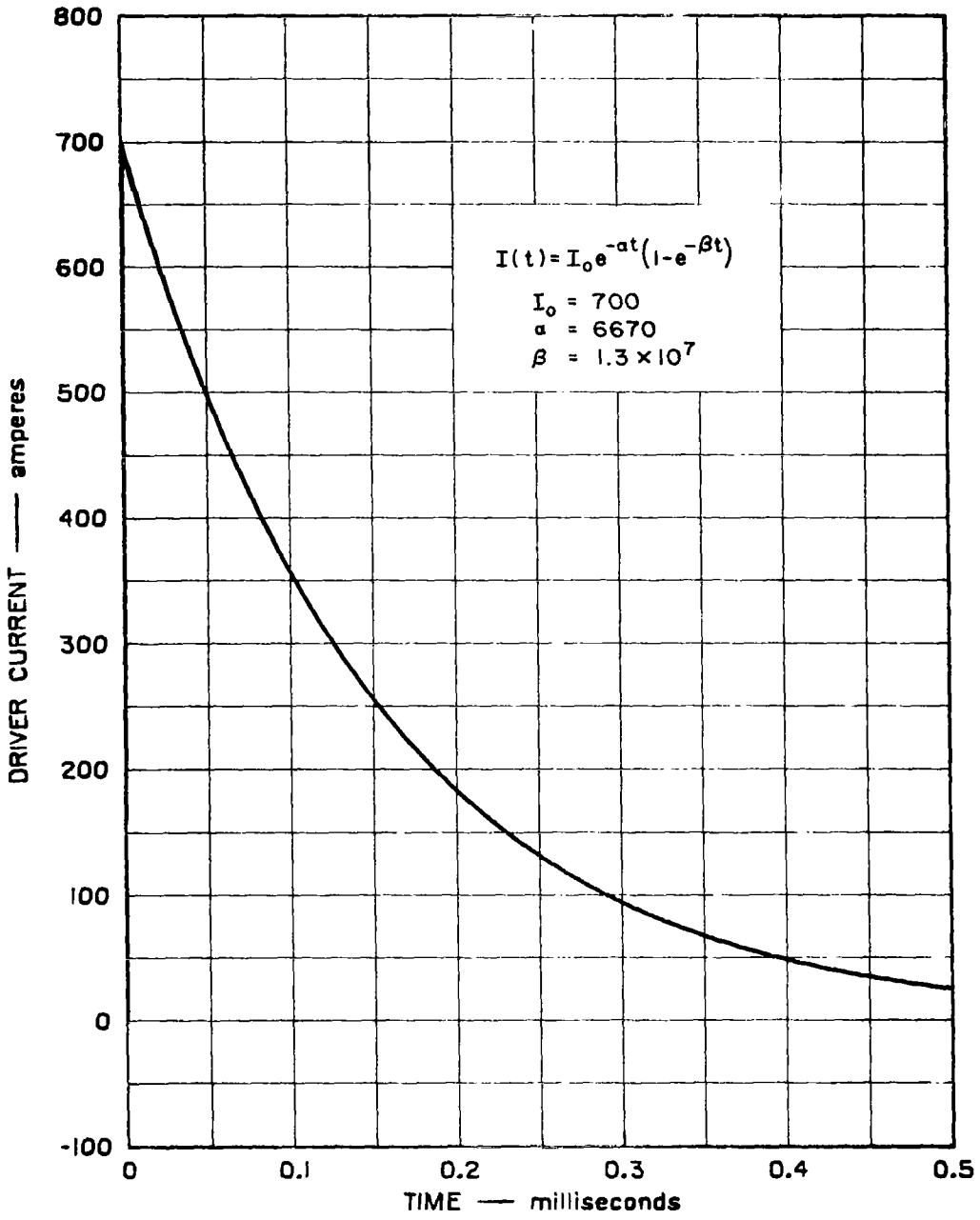

FIG. 5 FORM OF CURRENT PULSE USED TO DRIVE OUTER SHIELD

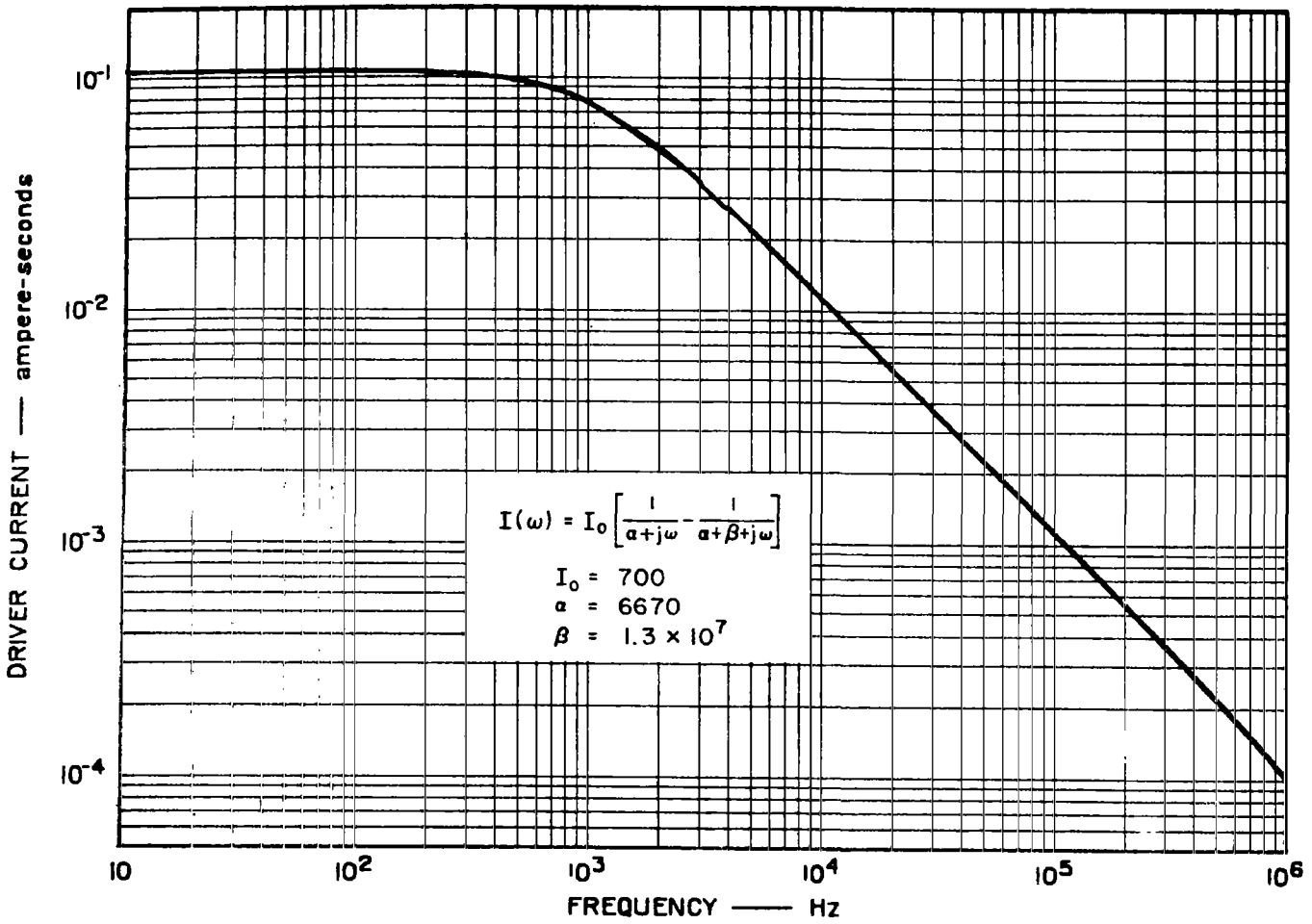

FIG. 6 CURRENT SPECTRUM OF PULSE USED TO DRIVE OUTER SHIELD

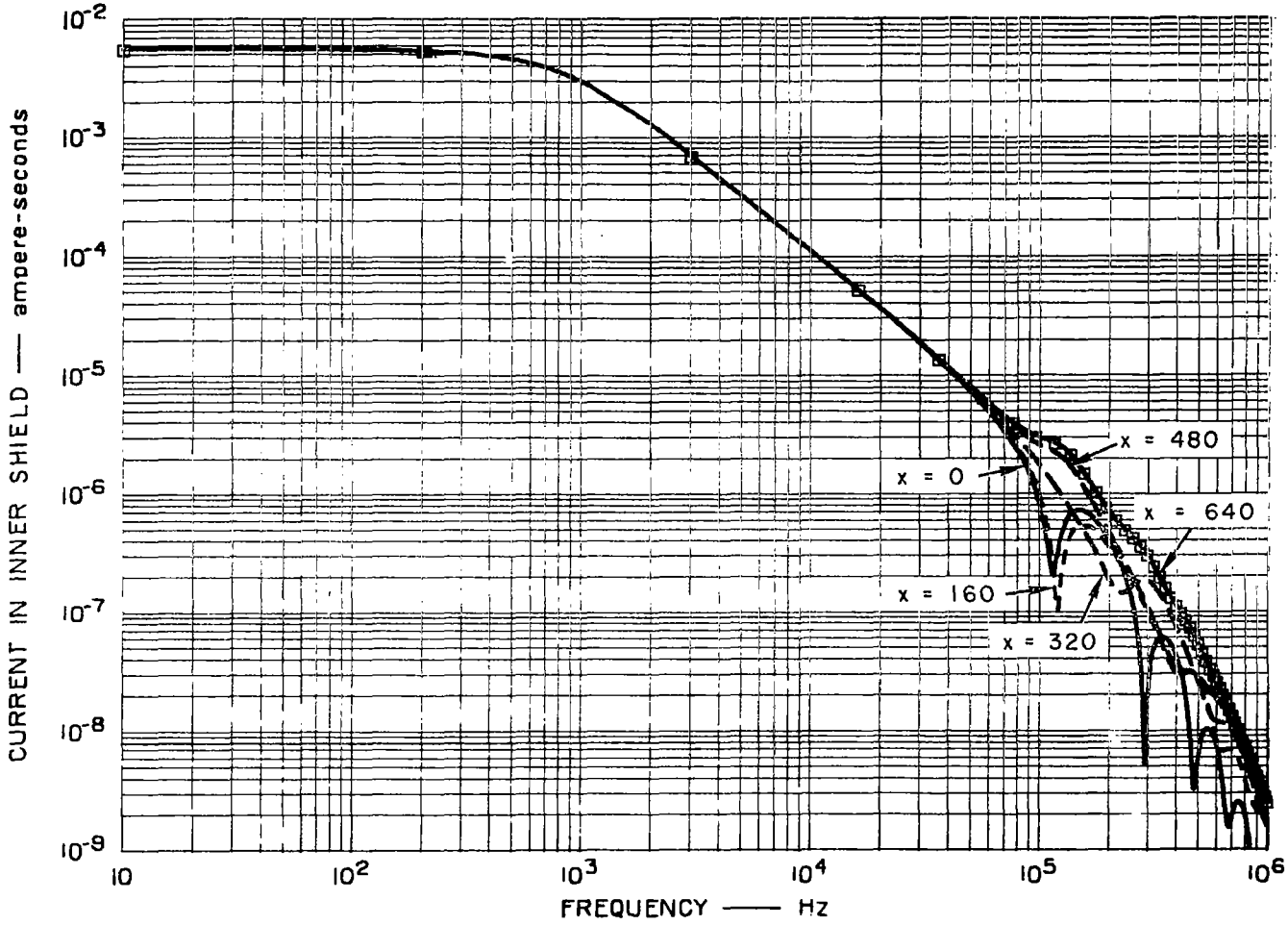

FIG. 7 SPECTRA OF CURRENT IN INNER SHIELD WHEN OUTER SHIELD IS DRIVEN WITH PULSE OF FIG. 5 — SHIELDS ARE SHORTED AT x = 0 AND AT x = 640 METERS

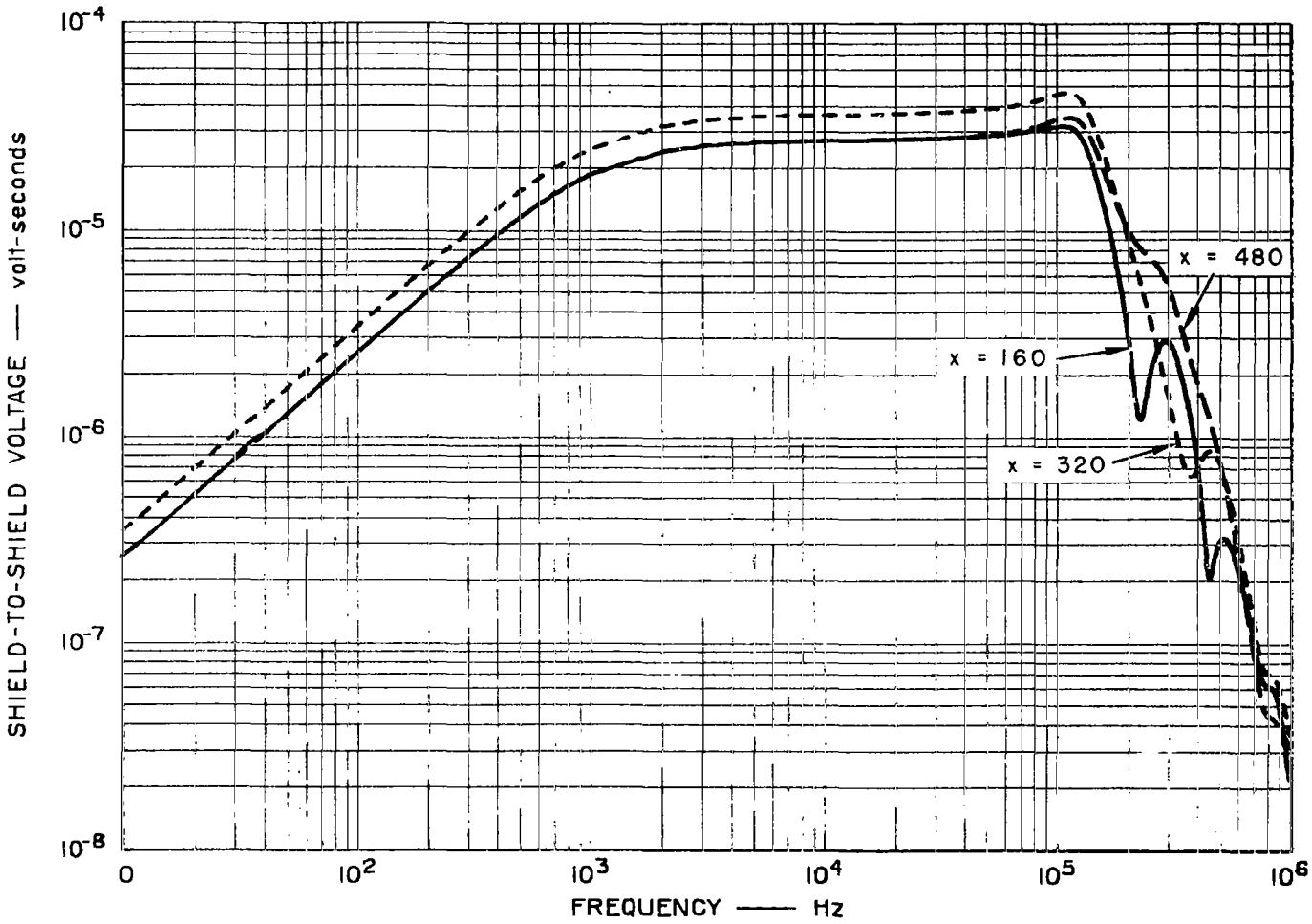

FIG. 8 SHIELD-TO-SHIELD VOLTAGE SPECTRA WHEN OUTER SHIELD IS DRIVEN WITH PULSE OF FIG. 5 — SHIELDS ARE SHORTED AT x = 0 AND AT x = 640 METERS

frequencies below 50 kHz, and at the higher frequencies where significant differences occur, the magnitude of the spectrum is more than 60 dB below the low-frequency amplitude. The inverse Fourier transforms of the current spectra of Fig. 7 are shown in Fig. 9. The current pulses at all five points along the cable are identical on the scale of Fig. 9. The pulse shape of Fig. 9 is also in good agreement with the shape measured in the experiments on the 640m test cable.

The sheath-to-sheath voltage spectra shown in Fig. 8 are similar in shape below 100 kHz, but show significant deviations above 100 kHz because of resonance or standing-wave effects. Because the resonance differences occur at spectral levels within 30 dB of the maxima of the spectra, they influence the shape of the pulses in the time domain. The voltage pulses in the time domain, obtained from the inverse transforms of the frequency spectra, are shown in Fig. 10 for all five points along the cable. Note that at the end points these pulse amplitudes are zero, and that the amplitude is greatest at the midpoint. The pulse appears to be a 100 kHz damped oscillation. This is approximately the natural frequency of the shield-to-shield transmission line in the half-wave mode. (The phase factor in this line is almost twice that of free space because of the dielectric and the low Q of the line at these frequencies.) No experimental shield-to-shield voltage data were taken for comparison with the results of Fig. 10.

To carry the analysis through the inner shield to the core, the current in the inner sheath as defined by Fig. 9 (or Fig. 7) was assumed to propagate down the inner shield with the propagation velocity characteristic of the shield-to-shield transmission line. The axial field produced at the inside surface of the inner shield by this current was then used in the transmission-line equations to compute the core current and the core-to-sheath voltage. It should be noted, however, that this technique is satisfactory only if the current in the inner sheath is essentially independent of position along the cable (as was the case here), or if the passband of the inner shield is such that only the quasistatic components penetrate the inner sheath. That is, if the axial field along the inside surface of the inner shield is not of uniform

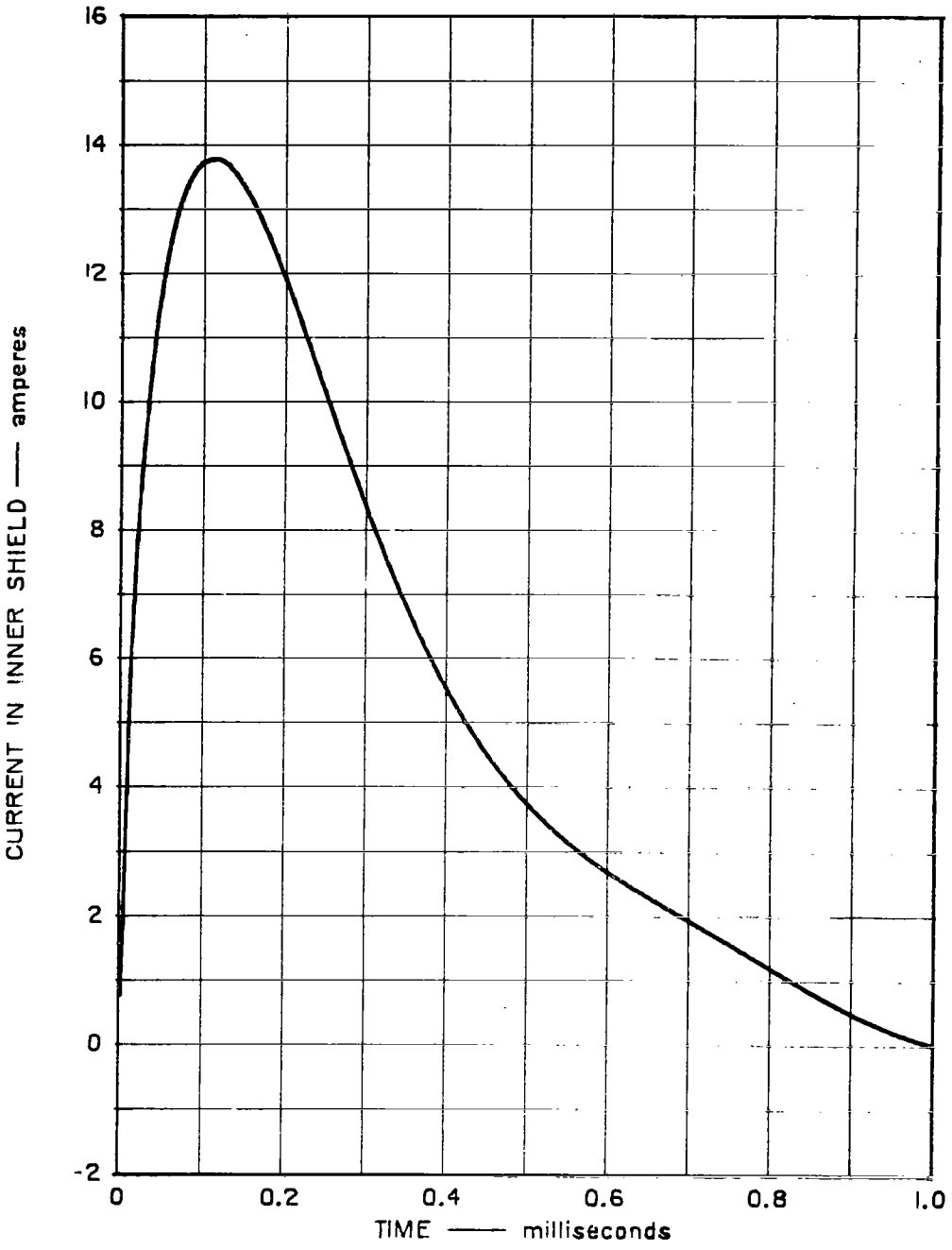

FIG. 9 CURRENT PULSE IN INNER SHIELD WHEN OUTER SHIELD IS DRIVEN WITH PULSE OF FIG. 5 (inverse transform of spectra of Fig. 7)

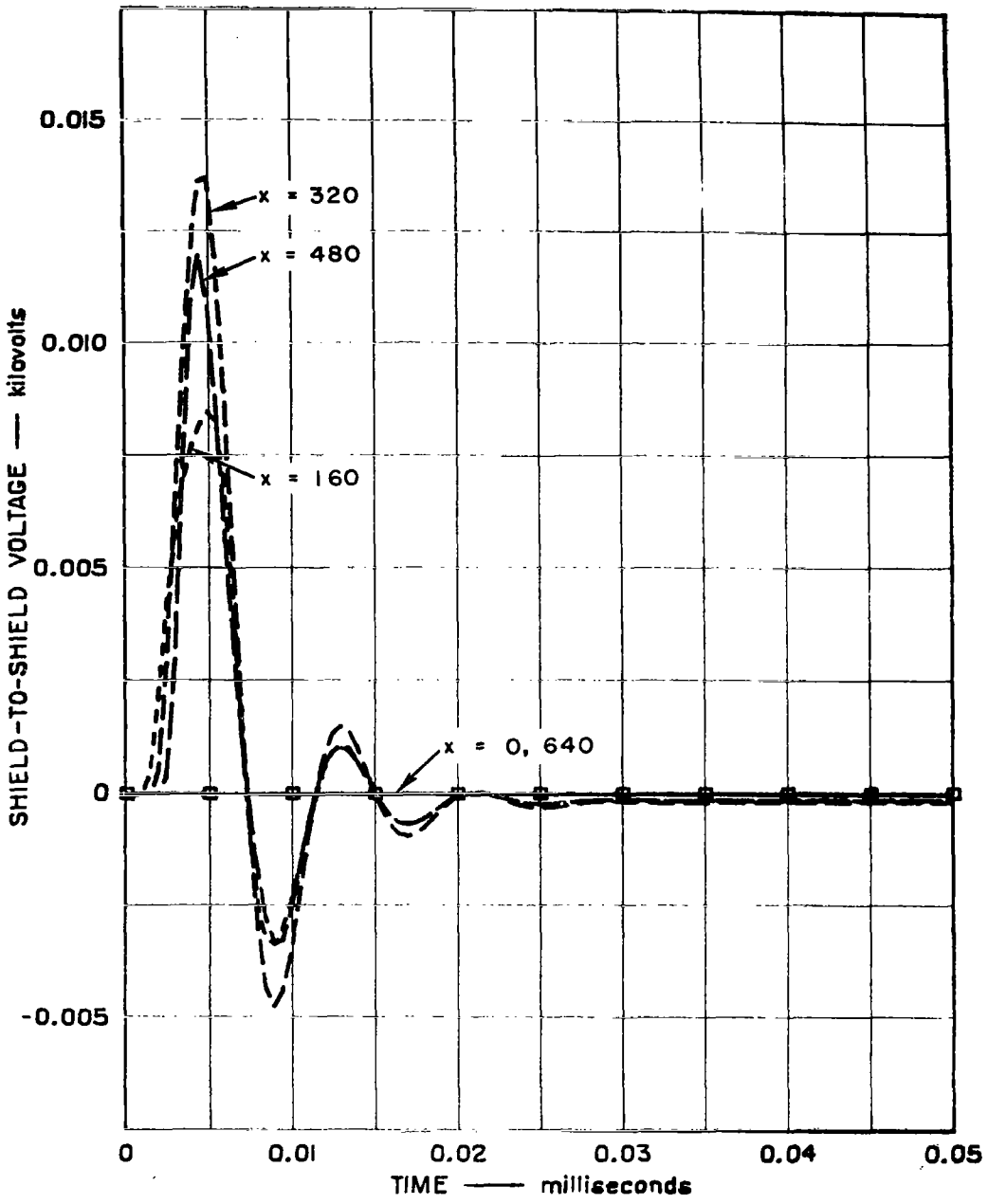

FIG. 10 SHIELD-TO-SHIELD VOLTAGE PULSES WHEN OUTER SHIELD IS DRIVEN WITH PULSE OF FIG. 5 (inverse transform of spectra of Fig. 8)

amplitude and essentially in phase along the entire length of the cable, this field must be treated as a variable in the integral of Eq. (14). (The same conditions apply to the outer sheath, but in the examples described here, the driving current was assumed to be unattenuated in propagating down the outer shield. The amplitudes are therefore independent of position along the line, and the phase is accounted for by the phase of the unit-impulse spectrum.)

The core-current spectra computed by this technique are shown in Fig. 11 for experimental driving current in the outer shield. The core-current spectra in this case are similar to the unit-impulse current spectra (see Fig. 3), since the experimental driving-current spectrum is similar to the impulse spectrum over the passband of the shield system. The core-current pulses in the time domain are shown in Fig. 12 for the five points along the cable (at the ends of the cable, the current is zero because of the open-circuit terminations). The current-pulse shapes are very similar to those measured in the cable experiment, and the computed amplitudes are in reasonable agreement with the measured amplitudes, considering that the actual core was comprised of 52 insulated conductors instead of the solid copper cylinder assumed in the computations.

The core-to-shield voltage spectra are shown in Fig. 13, and the voltage pulses are shown in Fig. 14. As the figures show, the voltage is skew-symmetric about the midpoint of the cable, with the maximum voltage appearing at the ends. The computed voltage peak is 22V at the ends for a 700A peak driving current. The core-to-shield voltages measured in the experimental program for this driving current were 14V to 22V peak, and the pulse shapes were very similar to those of Fig. 14.

VII CONCLUSIONS

The techniques described here, together with the associated computer programs, are believed to be adequate to describe the internal currents and voltages in complex cable systems. The simplified techniques used in the examples described above are adequate for short cables (less than 5000M) if a uniform driving current in the outer shield is applicable.

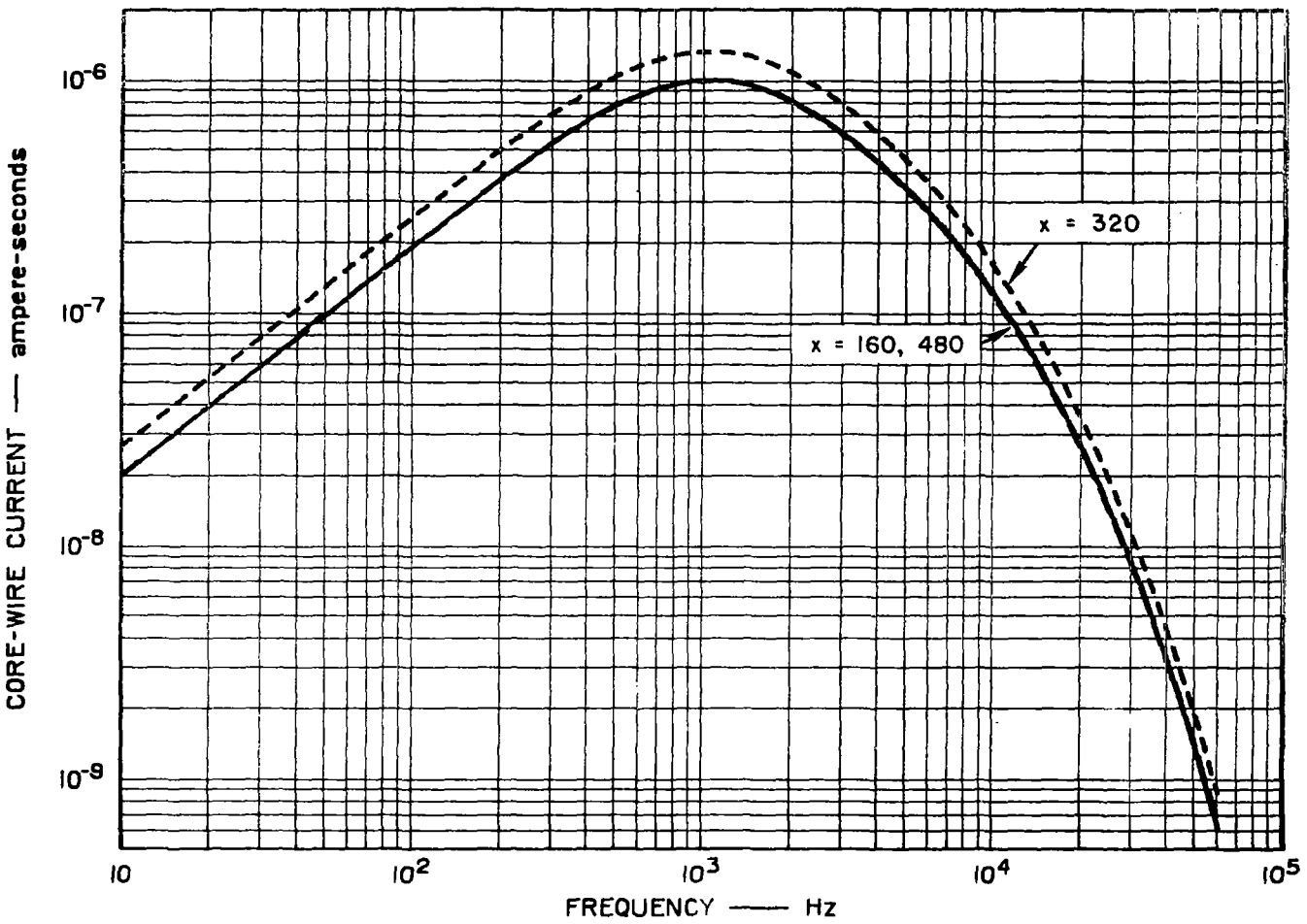

FIG. 11 CORE-CURRENT SPECTRA WHEN OUTER SHIELD IS DRIVEN WITH PULSE OF FIG. 5 — OPEN-CIRCUIT CORE-TO-SHIELD TERMINATION AT x = 0 AND AT x = 640 METERS

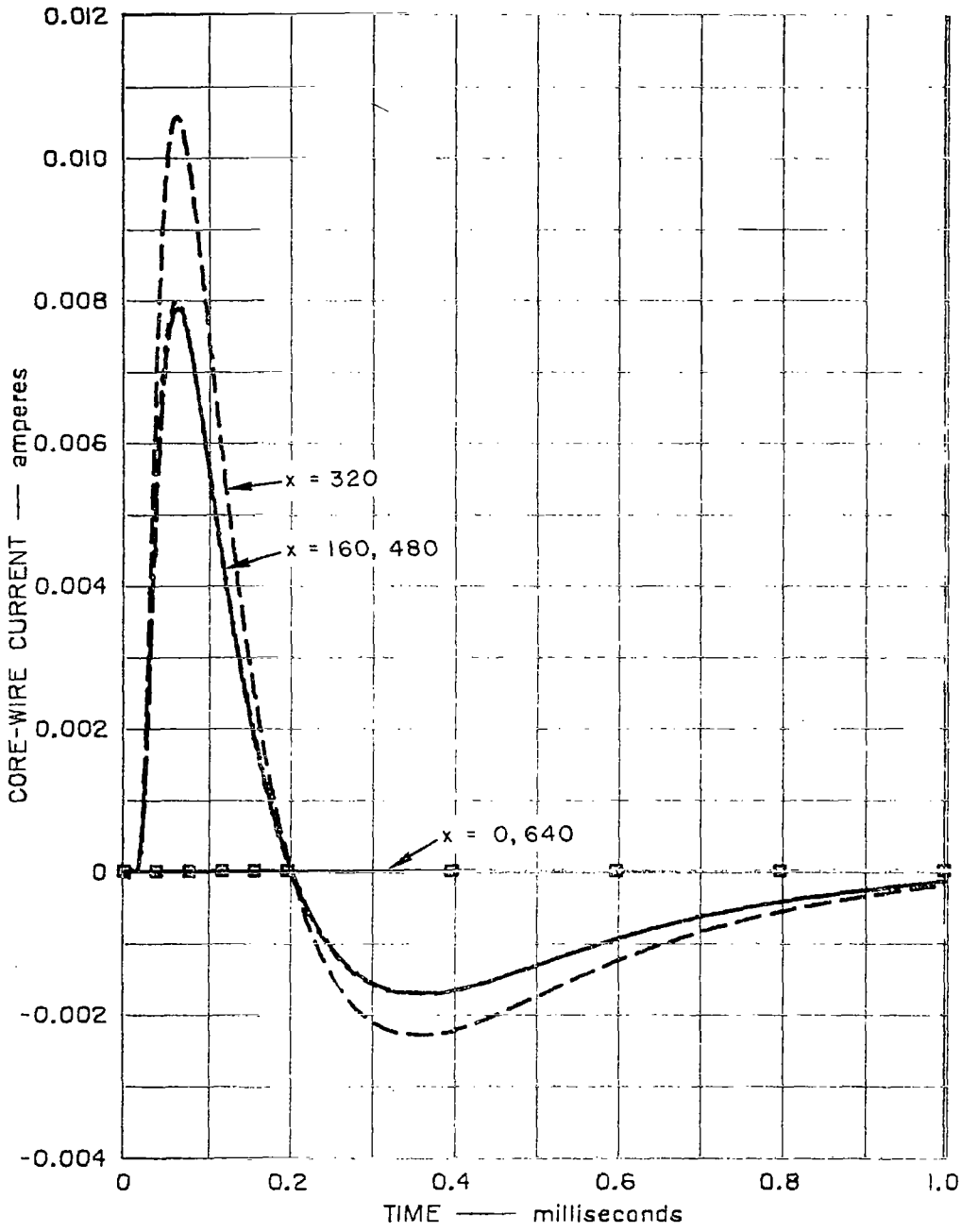

FIG. 12 CORE-CURRENT PULSE WHEN OUTER SHIELD IS DRIVEN WITH PULSE OF FIG. 5 (inverse transform of spectra of Fig. 11)

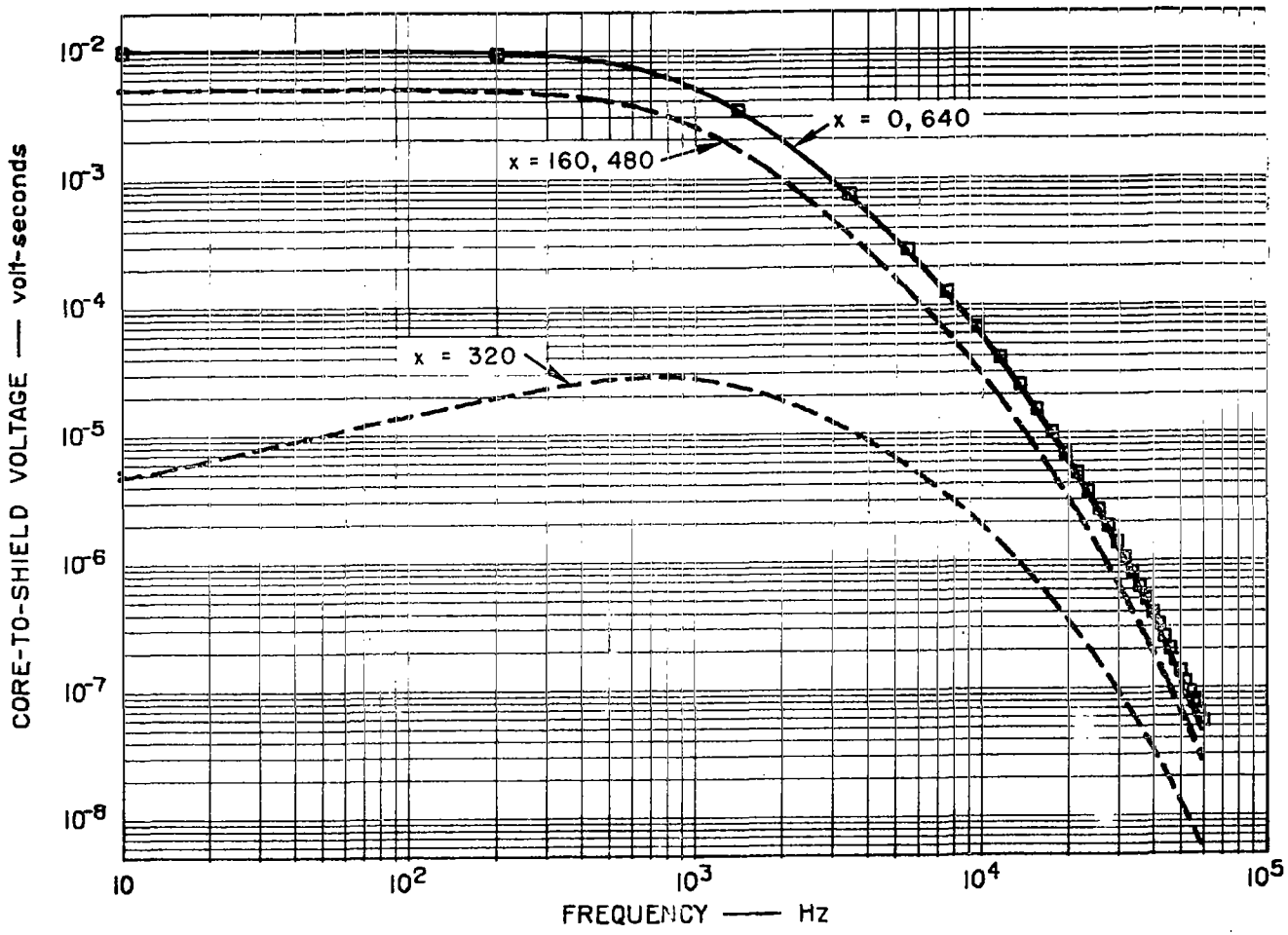

FIG. 13 CORE-TO-INNER-SHIELD VOLTAGE SPECTRA WHEN OUTER SHIELD IS DRIVEN WITH PULSE OF FIG. 5 — OPEN-CIRCUIT CORE-TO-SHIELD TERMINATION AT x = 0 AND AT x = 640 METERS

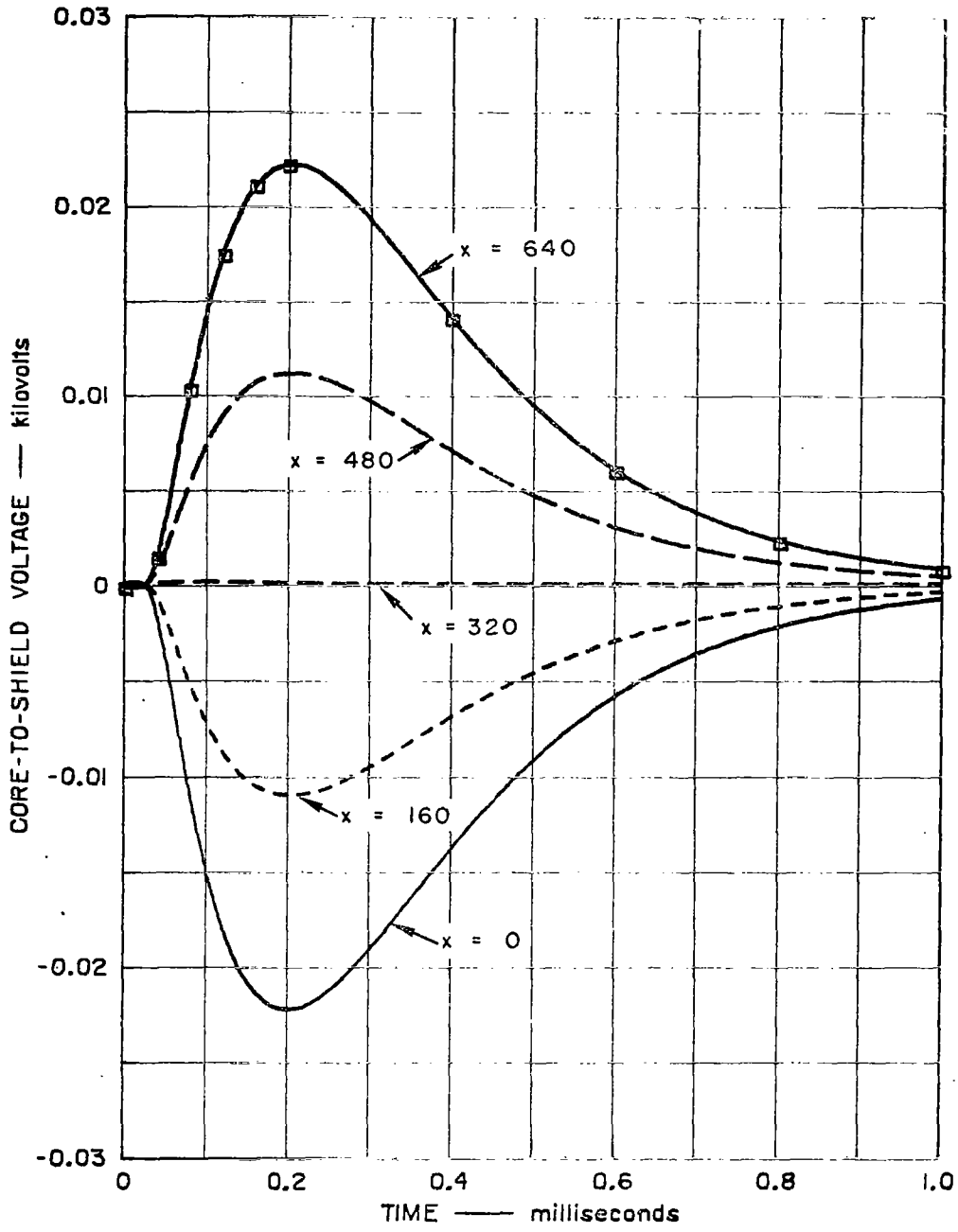

FIG. 14 CORE-TO-INNER-SHIELD VOLTAGE PULSE WHEN OUTER SHIELD IS DRIVEN WITH PULSE OF FIG. 5 (inverse transform of spectra of Fig. 13)

For longer cables or nonuniform driving currents, an additional numerical integration is necessary, which adds considerably to the computer time required. Much insight into cable problems can be gained, however, by studying the simpler cases such as the example analyzed above. The ability to compute pulse shapes and amplitudes that compare well with those obtained experimentally provides the confidence in the analytical approach that is needed to proceed to more complicated systems.

Appendix

IMPEDANCE AND ADMITTANCE FORMULAS

To use the transmission-line equations, it is necessary to compute the impedance per unit length and the admittance per unit length of the line. The properties of the line may be computed from available formulas for the internal impedance of cylindrical conductors and the inductance and capacitance of coaxial cylinders.

For coaxial cylinders, the impedance per unit length may be expressed as the sum of three components: the internal impedance of the outer conductor, the inductive reactance of the gap between the conductors, and the internal impedance of the inner conductor. The internal impedance of the inner conductor can be obtained from Eqs. (3) and (4) for tubular conductors:

$$Z_i = -\frac{(1-j)}{2\pi r_0 \sigma\delta}\left[\frac{H_1^{(1)}(\rho_i)\,J_0(\rho_0) - H_0^{(1)}(\rho_0)\,J_1(\rho_i)}{H_1^{(1)}(\rho_i)\,J_1(\rho_0) - H_1^{(1)}(\rho_0)\,J_1(\rho_i)}\right] . \qquad \text{(A-1)}$$

If the inner conductor is solid, ρ_i is zero and Eq. (A-1) reduces to

$$Z_i = -\frac{(1-j)}{2\pi r_0 \sigma\delta}\left[\frac{J_0(\rho_0)}{J_1(\rho_0)}\right] \qquad \text{(Solid)} \quad . \qquad \text{(A-2)}$$

The internal impedance Z_i of the outer conductor is obtained by interchanging ρ_i and ρ_0 in Eq. (A-1) for a tubular conductor:

$$Z_e = \frac{(1-j)}{2\pi r_i \sigma\delta}\left[\frac{H_1^{(1)}(\rho_0)\,J_0(\rho_i) - H_0^{(1)}(\rho_i)\,J_1(\rho_0)}{H_1^{(1)}(\rho_0)\,J_1(\rho_i) - H_1^{(1)}(\rho_i)\,J_1(\rho_0)}\right] . \qquad \text{(A-3)}$$

If the outer conductor is solid (e.g. for a cable buried at a large depth in the soil), $\rho_0 \to \infty$ and Eq. (A-3) becomes

$$Z_e = - \frac{j\Gamma}{2\pi r_i \sigma} \left[\frac{H_0^{(1)}(\rho_i)}{H_1^{(1)}(\rho_i)} \right] \quad \text{(Solid)} \quad . \qquad \text{(A-4)}$$

Since the principal application of Eq. (A-4) is where the soil is the outer conductor, it will be necessary (in some cases) to include the displacement current in the internal-impedance calculation by substituting

$$\sqrt{-j\omega\mu(\sigma + j\omega\epsilon)} \quad \text{for} \quad - \frac{1 - j}{\delta} \qquad \text{(A-5)}$$

in determining ρ_i and δ in Eq. (A-4).

The inductive reactance of the gap between the conductors is

$$Z_g = j \frac{\omega\mu_0}{2\pi} \ln \frac{r_0}{r_1} \qquad \text{(A-6)}$$

where r_0 and r_1 are the inside radius of the outer conductor and the outside radius of the inner conductor, respectively.

The impedance per unit length applicable to Eqs. (10) et seq. is thus the sum of the three component impedances:

$$Z = Z_i + Z_e + Z_g \qquad \text{(A-7)}$$

When both the inner and outer conductors are good conductors (metal), the admittance per unit length is simply the capacitive reactance per unit length of the gap:

$$Y = Y_g = j\omega C = j \frac{2\pi\omega\epsilon}{\ln(r_0/r_1)} \quad . \qquad \text{(A-8)}$$

If dielectric loss is important, the permittivity ϵ in Eq. (A-7) is complex:

$$\epsilon = \epsilon'(1 - j \tan\delta_e) \qquad \text{(A-9)}$$

where $\tan\delta_e$ is the loss tangent for the dielectric in the gap.